Curved infrared screens

A. Banerjee,[1] D. Sliwinski,[1] K. P. Stewart,[2] K. D. Möller,[1] and H. Grebel[1,*]

[1]*Electronic Imaging Center and Electrical Engineering Department, New Jersey Institute of Technology, Newark, New Jersey 07102, USA*

[2]*Naval Research Laboratory, 4555 Overlook Avenue, SW, Washington, DC 20375-5351, USA*

**Corresponding author: grebel@njit.edu*

Received November 16, 2009; accepted March 22, 2010;
posted April 9, 2010 (Doc. ID 119991); published May 6, 2010

We address curved IR screens for multiwavelength systems. To first-order of the approximation, a curved screen may be viewed as composed of many local flat screens. On the other hand, the validity of such an approximation is not clear *a priori*. We provide experiments and simulations to show that such an approximation works well for cylindrically curved IR screens while monitoring their peak transmission as a function of the screen curvature. © 2010 Optical Society of America

OCIS codes: 050.6624, 240.6680, 260.3060, 290.3700.

Free-standing thick metal screens, with the ratio of thickness to periodicity constant larger than 0.1, have been studied for quite some time [1]. In general, periodic metallo–dielectric structures are able to discriminate desired IR signals from more energetic short wavelength radiation, allow color temperature measurements, provide order sorting for grating spectrometers, and improve the signal-to-noise ratio of Fourier transform spectrometers. Square-shaped freestanding metal screens are commercially available and have been used as bandpass filters [2], reflectors for long IR wavelengths, Fabry–Perot etalons [3], and antennas [1]. In principle, such flat periodic structures enable transmission (or reflection) of specific IR bands by invoking standing wave surface modes: the incident beam is coupled to the surface waves by the periodic structure, which in turn supports standing waves [4]. The standing waves on both sides of the screen are coupled through waveguide modes in the structure opening.

Curved frequency selective surfaces for the microwave region have been proposed in the past [5–7]. Yet, most available simulation tools fall short on these structures: one cannot take advantage of periodic boundary conditions as typically made with their flat screen counterparts. In order to simplify calculations, a typical approximation used is to divide the curved surface into many planar sections. Such an approximation does not adequately predict the transmission through curved microwave structures [7]. With a standing wave picture in mind, a related question is what the minimal size of the planar segment should be in order for the approximation to be valid.

Here we consider curved IR screens. There are a few differences between the microwave and IR applications: the wavelength of the IR is much shorter; thus, even a small planar segment extends through many IR wavelengths; a screen is considered thick when its thickness t exceeds 0.1 of its resonance wavelength. Therefore, most of the microwave screens are considered *thin*, whereas our IR screens are thick (screen thickness/resonance wavelength $\sim 1/3$); the spectral region covered in the IR is much larger than the bandwidth covered by a typical microwave antenna; there is a merit for considering such screens in the IR: photons are scarce in this spectral region and increasing the collecting surface area directly affects the signal-to-noise ratio, since the signal is built up coherently by the resonating structure; and, finally, surface standing waves in the IR wavelength region may be useful for near-field applications as well [8–10].

Our approach is to consider these cylindrically curved screens as consisting of many locally flat screens, tilted at varying angles with respect to the collimated incident beam (Fig. 1). This approach is quite intuitive and is substantiated below. Much insight has been gained in dealing with flat and tilted screens for various polarizations [4] and we will utilize it here.

Free-standing (inductive) copper screens are commercially available from Precision Eforming. The screens have square openings of 7.6 μm $\times$ 7.6 μm, arranged in a square lattice with a 12.7 μm pitch. The screen thickness was 4 μm. The screens were mounted on a special fixture in a Fourier transform IR (FTIR) spectrometer so that its corresponding radius of curvature R was precisely assessed (Fig. 1). The polarization state of the incident beam was determined by an IR polarizer. Typically, peak splitting occurs in these spectrometers even when the screen is placed flat at normal incidence [4]. Simulations for flat and tilted screens have been made using Ansoft

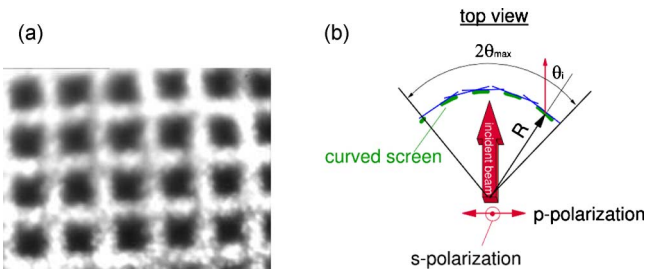

Fig. 1. (Color online) (a) Flat metal screen: 7.6 μm $\times$ 7.6 μm opening, arranged in a square lattice with a 12.7 μm pitch. (b) A cylindrically curved screen may be constructed by many flat yet tilted screens. R is the radius of screen curvature. The maximum azimuthal angle is θ_{max}. The local incident angle for this flat section is θ_i.

0146-9592/10/101635-3/$15.00

HFSS and CST commercial packages; unfortunately, commercial packages cannot simulate curved structures effectively.

Experimental data for a flat screen at various tilt angles are shown in Fig. 2. The transmissions for p-polarization (p-pol—the E-field oscillation is in the plane of incidence) and s-polarization (s-pol—the E-field oscillation is perpendicular to the plane of incidence) states of a collimated incident beam are shown in the figure. As can be seen from Figs. 2(a) and 2(b), the scattered p-pol beam tends to split: the wavelength difference between the peaks becomes larger as the tilt angle increases. The s-pol tends to remain as a single peak; however, it is shifted toward the lower frequencies. Simulations, made with both HFSS and CST commercial codes agree well with the experimental results for tilt angles different from zero. As shown in Fig. 3(a), the frequency splitting of the p-pol incident beam is evident. Yet, the dip exhibited by the experiment at normal incidence is missing. One may plot the peak frequency as a function of the tilt angle. This provides us with the dispersion relations plotted in Fig. 3(b).

Experimental transmission data for a *curved* screen as a function of its curvature angle $\theta_{\max}$ are shown in Fig. 4. As stated above, curved screens retain many of the features of flat screens measured at oblique incidence. Peak splitting is observed for p-polarized incident beams [Fig. 4(a)] and small peak shifting is observed for s-polarized incident beams [Fig. 4(b)]. Small variations between the peaks for s- and p-pol's at $\theta=0°$ may be explained by local screen deformations. Selective IR transmission through flat and tilted screens is the result of resonance conditions for the related surface plasmons (SPs).

Tilted flat screens: The SP wave with a wave vector k_{sp} is excited with the help of the periodic structure of the screen through the momentum conservation rule,

$$\mathbf{k}_{\mathrm{sp}} = \mathbf{k}_o \sin\theta + q\mathbf{G}. \tag{1}$$

Here, $\mathbf{k}_o \sin\theta$ is the projection of an incident wavenumber $\mathbf{k}_o$ on the screen surface, $\mathbf{G}$ is the reciprocal wave vector of the screen, and q is an integer. There are two counterpropagating surface waves for a given frequency, when taking into account translation symmetry with respect to $\mathbf{G}$ and folding symmetry of the Brillion zone (basically stating that $|\mathbf{k}_{\mathrm{sp}}-\mathbf{G}|=k_{\mathrm{sp}}$). These constitute standing surface modes, which enables the transmission (or, in some cases, reflection)

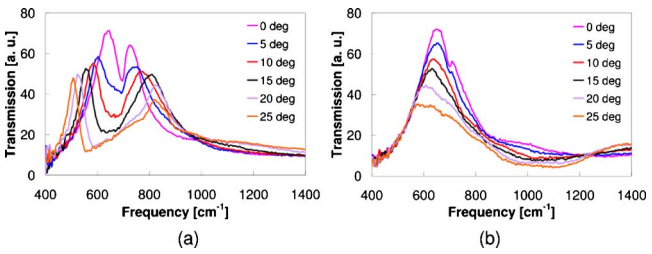

Fig. 2. (Color online) Experiment (curves are ordered from top to bottom): flat tilted screens. (a) p-polarized incident beam. (b) s-polarized incident beam. The dip in (a) at $\theta=0$ results from noncollimated incident beam [4].

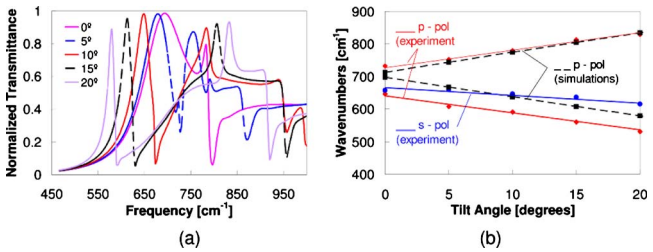

Fig. 3. (Color online) Simulations of tilted flat segments: (a) p-polarized incident beam (the dip as a function of tilt progresses sideways). (b) Dispersion relations for s- and p-pol's. The peak frequency is plotted as a function of the tilt angle. Experiment, p-pol: red (top and bottom solid linear best fit lines); experiment, s-pol: blue (second solid linear best fit line); simulations, p-pol: black (dashed linear best fit line). The noncollimated IR beam may diverge differently in p and s directions.

of a particular IR band. The last two equations are consistent if the Bragg reflection of the surface mode is made with the second (or higher) order of $\mathbf{G}$.

At normal incidence, the excited SP mode in these metal screens is doubly degenerate. Resonance occurs for wavelengths approximately matching the periodicity constant of the screen [4]. As the screen is tilted with respect to the incident beam, this degeneracy is lifted and a frequency gap is formed, hence the peak splitting for a p-polarized incident beam. The s-polarized incident beam excites only the doubly degenerate component, hence the single transmission peak. The dispersion curve for the p-polarized incident beam has two branches. The s-polarized peak follows the lower branch of the p-polarized beam (Fig. 3). The peak frequency position for flat screens, which are tilted at an angle θ, may be approximated as

$$\omega = \omega_0[1 \pm C \sin(\theta)]. \tag{2}$$

The constant C is of order $\frac{1}{2}$.

Curved screens: As mentioned before, the curved screen may be viewed as constructed of flat locally tilted screens. Instead of a varying frequency gap for each segment of the screen, we define an averaged frequency gap $\langle\Delta\omega\rangle$ over all flat segments for angles $\theta_i < \theta_{\max}$ (Fig. 1),

$$\langle\Delta\omega\rangle = 2C\omega_0\Sigma_i \sin(\theta_i)/\Sigma_i\theta_i. \tag{3}$$

Conversely, if the frequency gap at a given tilt angle is $\delta\omega_\iota = \delta\omega(\theta_i)$, then the average will be written as

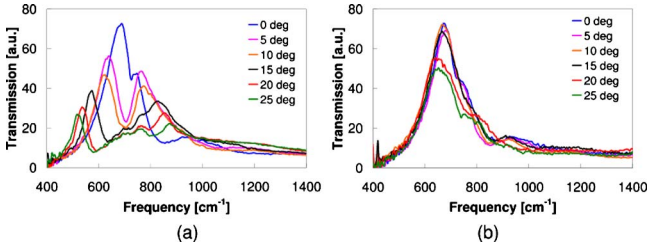

Fig. 4. (Color online) Transmission through cylindrically curved screens. (a) p-pol incident beam (as the curvature increases so does the frequency gap). (b) s-pol incident beam. The curvature is given in terms of $\theta_{\max}$. Curves are ordered from top to bottom.

$$\langle \Delta\omega \rangle = \Sigma_i \delta\omega_i / i. \quad (4)$$

In Fig. 5 we show the transmission frequency gap for the p-polarized incident beam as a function of the curvature angle θ_{max}. Based on Eq. (4), we divided the range from 0 to θ_{max} into 2° segments and calculated the averaged frequency gap for each curved screen. In Fig. 5 we compare the averaged experimental data for p-pol data with the averaged simulation data obtained by averaging flat and tilted screens. Typical spectrometers used focused beams instead of collimated ones for large throughputs: despite the non-collimation of the IR beam in the FTIR spectrometer, a qualitative agreement between this simple model and the experiment is observed. The constant shift of the experimental data is attributed to the non-collimated IR beam.

As stated before, at normal incidence, the excited SP mode in these metal screens is doubly degenerate and resonance occurs for wavelengths approximately matching the periodicity constant of the screen. Owing to presence of high-order harmonics [8] one expects that a small frequency gap would be opened even for $k=0$ (normal incidence). Most simulation tools fail to exhibit such a gap. The problem is complicated by the presence of noncollimated beam in IR spectrometers [4]. In order to assess the small gap at $k=0$, one may extend the linear fit for the simulated data at $\theta \neq 0$ back to the $\theta=0$ point. The overall frequency bandgap at $k=0$ is estimated at 15 cm^{-1} [Fig. 3(b)]. This result is also corroborated by the experimental data: we fitted the overall broadened peak by a few Gaussian curves and assessed the width of the major peak as a function of the tilt angle. As it turns out, the major peak at $k=0$ is wider than the peaks at other angles by more than 10 cm^{-1}.

Let us estimate the proper flat segment size, which maintains reasonable resonance conditions: the surface wavenumber for a perforated metallic surface may be written as $k_{sp}=k_0 n_{eff}=(\omega/c)n_{eff}$ with $n_{eff} \sim \sqrt{(\varepsilon_1\varepsilon_2/\varepsilon_1+\varepsilon_2)} \sim 1$. Coupled mode theory relates the coupling constant κ to the forbidden wavenumber range as $\kappa=|\delta k_{sp}|/2$, which in turn is related to the frequency gap as $\delta k_{sp}=(2\delta\omega/c)n_{eff}=(\Delta\omega/c)n_{eff}$; therefore, the coupling constant may be related to the entire frequency gap $\Delta\omega$ by $\kappa=(\Delta\omega/2c_n)$ with $c_n \sim c$. The entire frequency gap was $\Delta\omega \sim 15$ cm^{-1}; therefore, $\kappa = 7.5$ cm^{-1}. The coupling length for surface Bragg modes may be calculated through the surface mode reflection coefficient, $\tanh(\kappa L) \sim 1$, which dictates $\kappa L \geq 2$; a minimum coupling length is therefore 2/7.5 cm or 2.6 mm. This means that: (1) if a curved screen is approximated by flat segments, each segment should be at least 2.6 mm wide. Such a condition puts a limit on the radius of curvature of the screen. (2) Averaging 2° flat segments for a curvatures up to $\theta_{max}=30°$ (radius of curvature is 100 mm) is adequate. (3) Our segmented flat screen approach is justified for thick IR screens. The approach may not be justifiable for microwave structures unless a proper scaling is made.

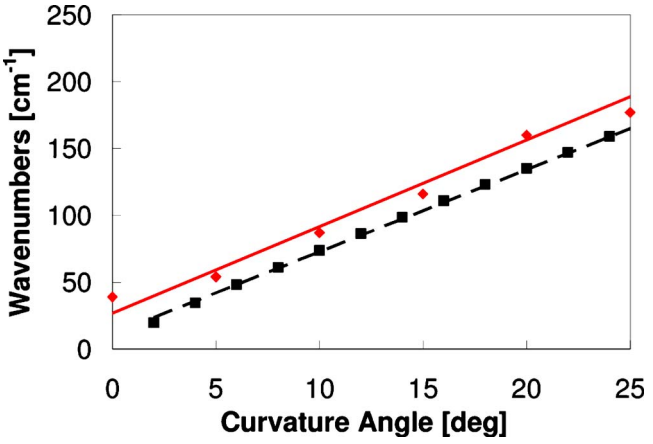

Fig. 5. (Color online) Frequency gap as a function of curvature angle θ_{max}. Red diamonds (with red linear trend line): experimental data for p-pol. Black squares (with dashed black linear trend line): simulations and use of Eq. (4).

In summary, curved IR screens for multiwavelength systems have been assessed. Many features of the cylindrically curved screens could be attributed to locally tilted segments of flat screens. The extension to spherical screens could be made in a similar way. Moreover, owing to the relatively local aspect of the resonating segments, the extension to a periodic structures may be made as well. Practical applications for these screens may be found in multipurpose imagers with frequency selectors (e.g., the reflected portion of the frequency band is used for imaging, and the transmitted band is used for IR filtering).

This project was funded in part by the National Science Foundation (NSF) IIS0514361. Support by the NCMR Program sponsored by the National MASINT Management Office (NMMO) is greatly appreciated.

References

1. B. J. Munk, *Frequency Selective Surfaces* (Wiley, 2000).
2. G. M. Ressler and K. D. Möller, Appl. Opt. **6**, 893 (1967).
3. R. Ulrich, K. F. Renk, and L. Genzel, IEEE Trans. Microwave Theory Tech. **11**, 363 (1963).
4. O. Sternberg, K. P. Stewart, Y. Hor, A. Bandyopadhyay, J. F. Federici, M. Bornefeld, Y.-L. Mathis, D. Sliwinski, K. D. Möller, and H. Grebel, J. Appl. Phys. **104**, 023103 (2008).
5. R. Mittra, C. H. Chan, and T. Cwik, Proc. IEEE **76**, 1593 (1988).
6. E. A. Parker, B. Philips, and R. J. Langley, IEEE Microw. Guid. Wave Lett. **5**, 338 (1995).
7. Z. Sipus, M. Bosiljevac, and J. Bartolic, in *2008 IEEE International Symposium on Antennas and Propagation and USNC/URSI National Radio Science Meeting, APSURSI 2008* (2008), p. 4619216.
8. R. Li, A. Banerjee, and H. Grebel, Opt. Express **17**, 1622 (2009).
9. A. Banerjee, D. Moeller, and H. Grebel, ECS Trans. **19**, 233 (2009).
10. A. Banerjee, D. Moeller, A. I. Smirnov, and H. Grebel, IEEE Sens. J. **10**, 419 (2010).